

subsequent O-to-N rearrangement via 1,4-addition of the serine nitrogen to the activated cyclohexenimine core (Fig. 3B). We favor this pathway, as it is consistent with the poor electrophilicity of mycosporine glycine (24); an alternative mechanism for Ava_3855 involving a direct condensation is detailed in scheme S3.

The in vitro characterization of Ava_3856 and Ava_3855 reveals two distinct, yet complementary, mechanisms of ATP-dependent enzymatic imine formation that differ from conventional chemical methods and biochemical mechanisms. These enzymes have evolved from peptide bond-forming catalysts in distinct ways: ATP-grasp homolog Ava_3856 generates a new type of electrophile using vinylogous acid activation, and NRPS-like enzyme Ava_3855 likely employs an unusual release mechanism. The recruitment of ATP-dependent peptide bond-forming enzymes in this manner is so far unprecedented in natural product biosynthesis and defines a new biosynthetic logic for imine construction. A short four-enzyme pathway thus converts a primary metabolite from the pentose phosphate pathway into a widely distributed class of small-molecule biological sunscreens using mechanistically elegant chemistry.

References and Notes

- C. S. Cockell, J. Knowland, *Biol. Rev. Camb. Philos. Soc.* **74**, 311 (1999).
- W. M. Bandaranayake, *Nat. Prod. Rep.* **15**, 159 (1998).
- J. M. Shick, W. C. Dunlap, *Annu. Rev. Physiol.* **64**, 223 (2002).
- A. Oren, N. Gunde-Cimerman, *FEMS Microbiol. Lett.* **269**, 1 (2007).
- W. C. Dunlap, J. M. Shick, *J. Phycol.* **34**, 418 (1998).
- E. J. Trione, C. M. Leach, J. T. Mutch, *Nature* **212**, 163 (1966).
- J. Favre-Bonvin, N. Arpin, C. Brevard, *Can. J. Chem.* **54**, 1105 (1976).
- B. Dehorter *et al.*, *Phytochemistry* **19**, 2311 (1980).
- P. J. Neale, A. T. Banaszak, C. R. Jarriel, *J. Phycol.* **34**, 928 (1998).
- N. L. Adams, J. M. Shick, *Mar. Biol.* **138**, 267 (2001).
- A. Oren, *Geomicrobiol. J.* **14**, 231 (1997).
- I. Yakovleva, R. Bhagooli, A. Takemura, M. Hidaka, *Comp. Biochem. Physiol. B* **139**, 721 (2004).
- F. de la Coba *et al.*, *J. Dermatol. Sci.* **55**, 161 (2009).
- J. Favre-Bonvin, J. Bernillon, N. Salin, N. Arpin, *Phytochemistry* **26**, 2509 (1987).
- A. Portwich, F. Garcia-Pichel, *Phycologia* **42**, 384 (2003).
- A. Starcevic *et al.*, *Proc. Natl. Acad. Sci. U.S.A.* **105**, 2533 (2008).
- Supporting information containing materials and methods, details of bioinformatics analyses, and assay data are available on Science Online.
- S. P. Singh, M. Klisch, R. P. Sinha, D.-P. Häder, *Genomics* **95**, 120 (2010).
- S. P. Singh, M. Klisch, R. P. Sinha, D.-P. Häder, *Photochem. Photobiol.* **84**, 1500 (2008).
- F. Lemoyne, J. Bernillon, J. Favre-Bonvin, M. L. Bouillant, N. Arpin, *Z. Naturforsch. C Biosci.* **40**, 612 (1985).
- S. L. Bender, S. Mehdi, J. R. Knowles, *Biochemistry* **28**, 7555 (1989).
- X. Wu *et al.*, *ChemBioChem* **8**, 239 (2007).
- T. Mahmud, P. M. Flatt, X. Wu, *J. Nat. Prod.* **70**, 1384 (2007).
- J. D. White, J. H. Cammack, K. Sakuma, *J. Am. Chem. Soc.* **111**, 8970 (1989).
- M. Y. Galperin, E. V. Koonin, *Protein Sci.* **6**, 2639 (1997).
- M. A. Fischbach, C. T. Walsh, *Chem. Rev.* **106**, 3468 (2006).
- T. Stachelhaus, H. D. Mootz, M. A. Marahiel, *Chem. Biol.* **6**, 493 (1999).
- This work was supported by a grant from the NIH (GM-20011). E.P.B. is the recipient of a NIH NRSA postdoctoral fellowship (GM-084625). We acknowledge Tri-K Industries (Northvale, NJ) for providing a sample of Helioguard 365 containing authentic standards of shinorine and porphyrin-334.

Supporting Online Material

www.sciencemag.org/cgi/content/full/science.1193637/DC1

Materials and Methods

Tables S1 to S5

Figs. S1 to S10

Schemes S1 to S3

References

11 June 2010; accepted 12 August 2010

Published online 2 September 2010;

10.1126/science.1193637

Include this information when citing this paper.

A General Mechanism for Network-Dosage Compensation in Gene Circuits

Murat Acar,^{1*†} Bernardo F. Pando,^{2*} Frances H. Arnold,³ Michael B. Elowitz,^{1,4} Alexander van Oudenaarden^{2,5}

Coping with variations in network dosage is crucial for maintaining optimal function in gene networks. We explored how network structure facilitates network-level dosage compensation. By using the yeast galactose network as a model, we combinatorially deleted one of the two copies of its four regulatory genes and found that network activity was robust to the change in network dosage. A mathematical analysis revealed that a two-component genetic circuit with elements of opposite regulatory activity (activator and inhibitor) constitutes a minimal requirement for network-dosage invariance. Specific interaction topologies and a one-to-one interaction stoichiometry between the activating and inhibiting agents were additional essential elements facilitating dosage invariance. This mechanism of network-dosage invariance could represent a general design for gene network structure in cells.

The number of copies of a gene network in a cell, or network dosage, has a direct effect on cellular phenotypes (1). Network dosage is altered in situations such as the switching

of some organisms between haploid and diploid life forms (2), doubling of chromosomes during cell cycle (3), genome-wide duplication of genetic content (4, 5), and global variation (6) in gene expression. Different phenotypes have different levels of sensitivity to such variations, and the need for effective compensation mechanisms arises when cells cannot tolerate these alterations.

It is believed that in the transition between haploid and diploid forms of life cells use a volume-mediated compensation mechanism to keep the concentrations of transcription factors constant as cell volume increases with ploidy (2). However, this mechanism cannot subdue the effects of global expression variation and genome duplication or loss events because they affect cellular

phenotypes independently of cell volume. For example, variability in ribosome numbers can cause substantial fluctuations in global expression levels. These observations raise the question of whether there are alternative layers of dosage compensation mechanisms independent of external factors such as cell volume. To what extent would network activity be robust to alterations in network dosage if we fixed cell volume and therefore excluded its compensatory effect? Could there be a molecular mechanism intrinsic to the network structure that helps cells diminish the effects of dosage variations? Despite the fundamental nature of these questions, what these mechanisms are and how they can be implemented has remained unclear.

With experimental and computational approaches, we investigate these questions by using the galactose signaling pathway (GAL pathway) of the yeast *Saccharomyces cerevisiae* as a model system (Fig. 1A). The GAL network has a well-characterized (7) bistable expression profile. Bistability (7–9) is a dynamical system property giving rise to two distinct gene expression states (off and on) for isogenic cells grown in the same environment. In a bistable gene network, the fraction of cells occupying the on state can be defined as the inducibility of the system and serves as a quantitative phenotypic trait. In the GAL network, four genes (*GAL2*, *GAL3*, *GAL4*, and *GAL80*) play key roles in regulating gene expression. The constitutively expressed Gal4p protein is a transcriptional activator that regulates expression of the other GAL pathway genes (10). Gal80p binds (11) to this protein and prevents Gal4p-mediated transcriptional activation. The protein Gal3p is activated (12) by galactose molecules that are imported into the cell by the galactose permease

¹Division of Biology, California Institute of Technology, Pasadena, CA 91125, USA. ²Department of Physics, Massachusetts Institute of Technology, Cambridge, MA 02139, USA. ³Division of Chemistry and Chemical Engineering and Division of Biochemistry and Molecular Biophysics, California Institute of Technology, Pasadena, CA 91125, USA. ⁴Howard Hughes Medical Institute and Department of Applied Physics, California Institute of Technology, Pasadena, CA 91125, USA. ⁵Department of Biology, Massachusetts Institute of Technology, Cambridge, MA 02139, USA.

*These authors contributed equally to this work.

†To whom correspondence should be addressed: E-mail: acar@caltech.edu

Gal2p. In its active form, Gal3p sequesters the Gal80p repressor to the cytoplasm, indirectly promoting transcription (13, 14). Except for the constitutive *GAL4* promoter, the activities of the different GAL pathway promoters are similar to each other (7). To quantify the activity of the GAL pathway at the single-cell level, we used the yellow fluorescent protein (YFP) driven by the *GAL1* promoter as our reporter and measured expression profiles at different galactose concentrations by using flow cytometry (Fig. 1, A and B). We interpreted these experimental results in the context of an effective model (15).

We observed similar inducibility profiles between haploid and diploid strains that contain the same reporter system (Fig. 2A), demonstrating that the system is invariant to ploidy changes. To dissect how network-dosage variations affect the

inducibility of the network in the absence of volume effects, we systematically reduced the number of copies of the four regulatory genes in the GAL network from two to one in diploid backgrounds by using *KanMX4* and *NatMX4* cassettes (15), obtaining 16 different diploid yeast strains, including the hemizygous and the wild-type strains that have all four genes at one and two copies, respectively (15).

Halving the dosage of *GAL3* dramatically reduced wild-type inducibility levels, whereas halving the dosage of *GAL80* made the cells need less galactose for full induction (Fig. 2B). Varying *GAL2* or *GAL4* dosage levels did not have a large effect on network activity (Fig. 2C).

To comprehensively explore the degree of dosage compensation in the GAL network, we measured the inducibility profiles of all 16 strains,

grouped the measurements in four dosage-perturbation orders, and compared the profiles to one another (Fig. 3A) (15). We observed similar inducibility profiles for the fourth-order hemizygous strain and the wild-type strain, implying the presence of network-dosage invariance in the GAL network, even in the absence of volume-mediated compensation effects (Fig. 3, A and B).

To determine the relative importance of each regulatory gene in affecting the wild-type inducibility levels, we quantified the average contribution of the second copy of each gene to inducibility (15). Figure 3C depicts the greater importance of *GAL3* as an activator and *GAL80* as an inhibitor compared with the relatively smaller contributions of *GAL2* and *GAL4* to the inducibility profiles (15). These results suggest that it may be possible to build a dosage-invariant network

Fig. 1. The galactose utilization pathway as a model gene network and bistability as a quantitative phenotype. **(A)** Gal3p* represents the galactose-bound, active form of Gal3p. The shuttling of Gal80p between the cytoplasm and the nucleus is denoted by the bidirectional red arrows. The dotted blue arrows show how the transcriptional feedback loops are established through Gal2p, Gal3p, and Gal80p. **(B)** Histograms show induction profiles of the wild-type galactose pathway for different galactose concentrations. a.u., arbitrary units.

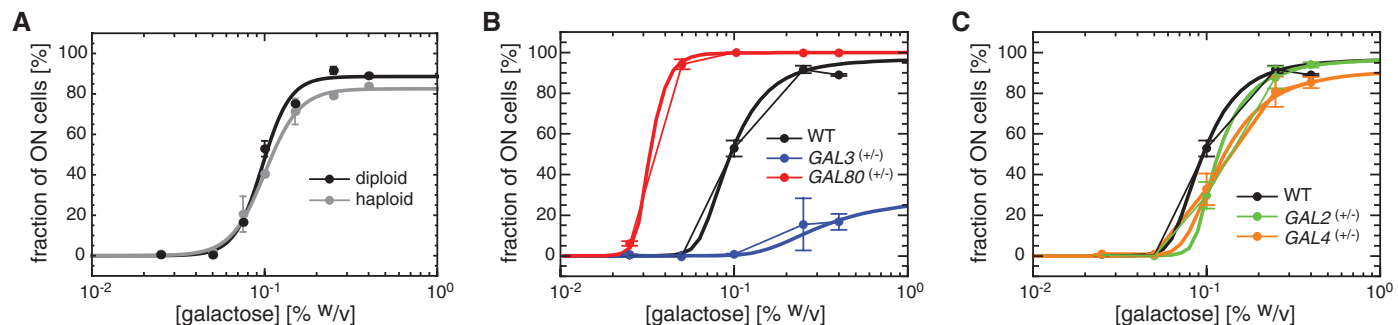
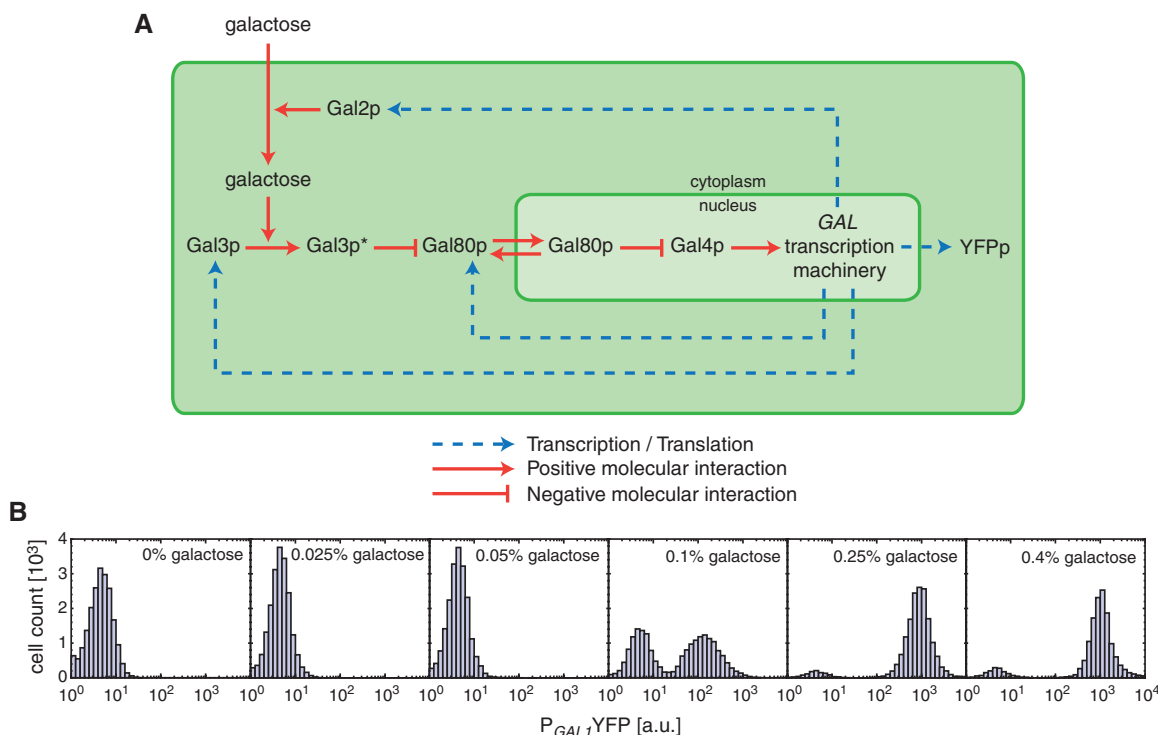
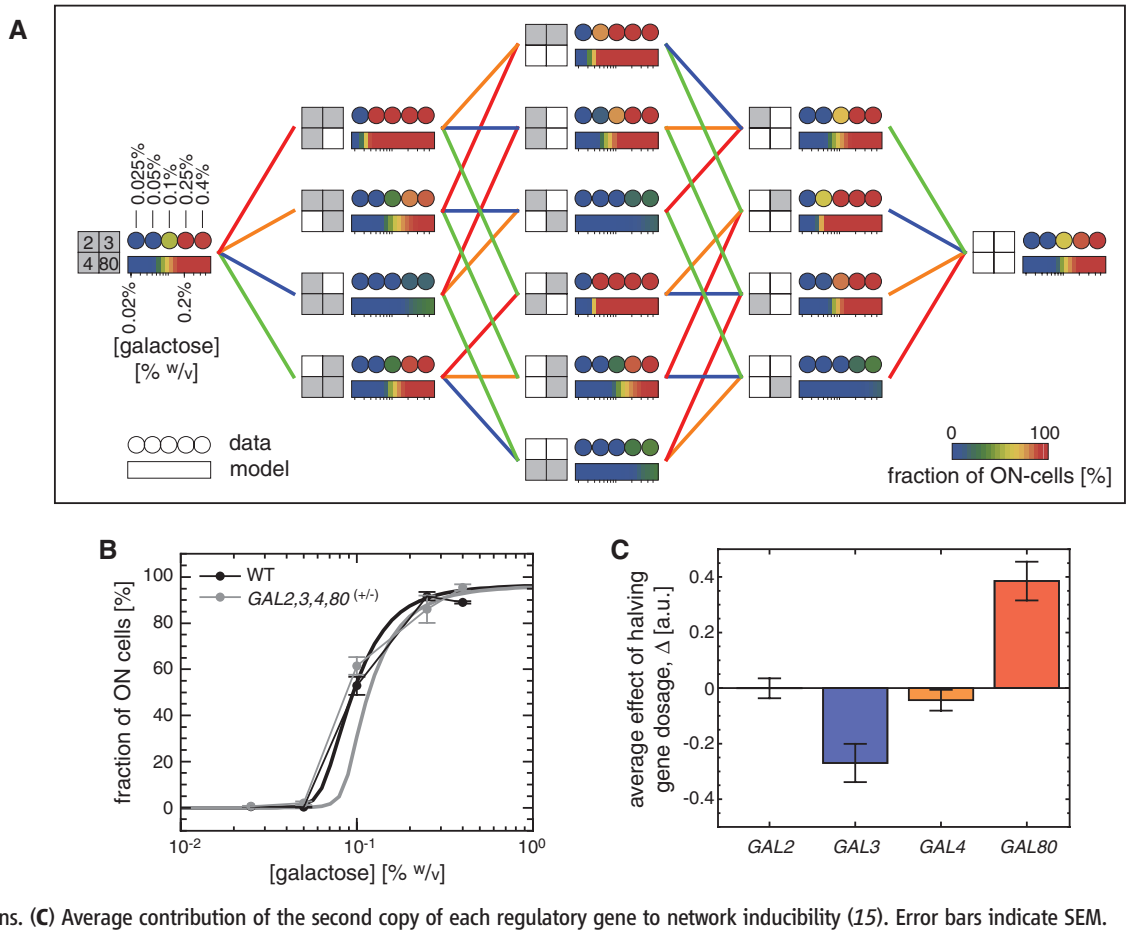


Fig. 2. Haploid-diploid comparison and measurement of the contribution of each regulatory gene to network inducibility. Error bars indicate SEM. **(A)** Fraction of on cells as a function of galactose concentration for both diploid and haploid strains. The solid lines are guides to the eye constructed by fitting a sigmoidal function to the data. **(B)** The inducibility profile of the GAL network

heterozygous in *GAL3* (blue) or *GAL80* (red) relative to the wild-type (WT) profile (black). **(C)** The inducibility profile of the GAL network heterozygous in *GAL2* (green) or *GAL4* (orange) relative to the wild-type profile (black). In both (B) and (C), the thick solid lines represent the model best fit to the five different inducibility profiles.

Fig. 3. Systematic dosage variations and network-dosage compensation. (A) The color of each circle represents the network inducibility level. The rectangular, color-coded bars reflect the predictions of the model based on the best fit to the data presented in Fig. 2, B and C. The genetic background of each strain is specified by a big square at its immediate left. The small squares represent the four regulatory genes of the GAL network. Gray color marks the presence of two copies of a specific gene, and white marks one copy of a specific gene. A line between two strains indicates that the two genetic backgrounds differ by a single copy of a specific gene, and the color of the line codifies that gene (blue for *GAL3*, red for *GAL80*, green for *GAL2*, and orange for *GAL4*). **(B)** The similarity between the inducibility profiles of the wild-type strain (black) and the strain containing one copy of each regulatory gene (gray). The thick solid lines represent the model predictions. **(C)** Average contribution of the second copy of each regulatory gene to network inducibility (15). Error bars indicate SEM.



by using only two components, but they do not by themselves indicate how the wiring topology of the network components contributes to network-dosage invariance.

To pinpoint the minimal general conditions that can facilitate dosage invariance in the absence of volume effects, we moved away from the specific case of the GAL pathway and analyzed generic network structures consisting of a set of genes all regulated by the same factor (15). We first found that any network with only one component cannot be dosage invariant. For networks with two components, dosage invariance is possible only if the components have opposite regulatory signs (i.e., if one is an activator and the other is an inhibitor).

To further explore how certain wiring topologies of the two-component generic networks would affect dosage invariance, we performed numerical investigations on the possible network topologies and analyzed their inducibility properties. Alternative network configurations are achieved on the basis of the following interaction topologies: the activator indirectly activates transcription, the activator directly activates transcription, the inhibitor gives up its direct-repressor role, and the activator assumes a direct-activator role (Fig. 4A). Each interaction topology is represented by a four-parameter functional form (Fig. 4A).

We randomly sampled the parameters characterizing these forms over large ranges and fed them into the quantitative model to obtain numerical inducibility curves corresponding to the networks carrying one or two copies of the network genes (15). For each pair of these numerical curves, we calculated the level of dosage invariance by quantifying the area between the two curves, large areas corresponding to large penalties to network-dosage invariance and vice versa (Fig. 4B). In principle, a high degree of dosage invariance can be observed at several different inducibility levels. For example, a biological network always staying in its off state is network-dosage invariant, but it lacks the ability to respond to signals of any kind. Thus, it is important to determine whether a dosage-compensated system is also inducible or not. We quantified the relative inducibility levels of our numerical curves relative to a reference induction profile. Large differences from the reference curve corresponded to large penalties to inducibility (Fig. 4B). An examination of the dot plots reveals that the topologies at left and right exhibit both dosage invariance and inducibility for a wide range of parameter sets. The specific interaction configuration in the two networks is essential for the systems to display such behavior (Fig. 4A). However, the choice between activator and inhibitor

in directly influencing transcription is not essential, so long as the other component regulates indirectly.

The green areas in Fig. 4B enclose the parameter sets corresponding to dosage-invariant and inducible networks (low penalties in both axes). For each point populating these areas, we extracted out the values of the four parameters (Fig. 4, C and D) (15). The parameter quantifying the nonlinearity of the interaction between the inhibiting and activating agents (α in Fig. 4C and β in Fig. 4D) was the only one severely restricted in its values, which displayed a narrow distribution centered around one. Thus, the effective stoichiometry of the interaction between the activating and inhibiting agents has to be close to one-to-one for a system that is both inducible and network-dosage invariant (15).

To understand why an inducible, network-dosage invariant system requires these specific interaction topologies and a one-to-one stoichiometry, consider how the system would respond to coordinated changes in the activator and inhibitor levels. For the system in the center of Fig. 4A, the output depends on independent contributions from the activator and the inhibitor. For compensation, the increase in the activator concentration would have to be exactly compensated by the down-regulation effect by the

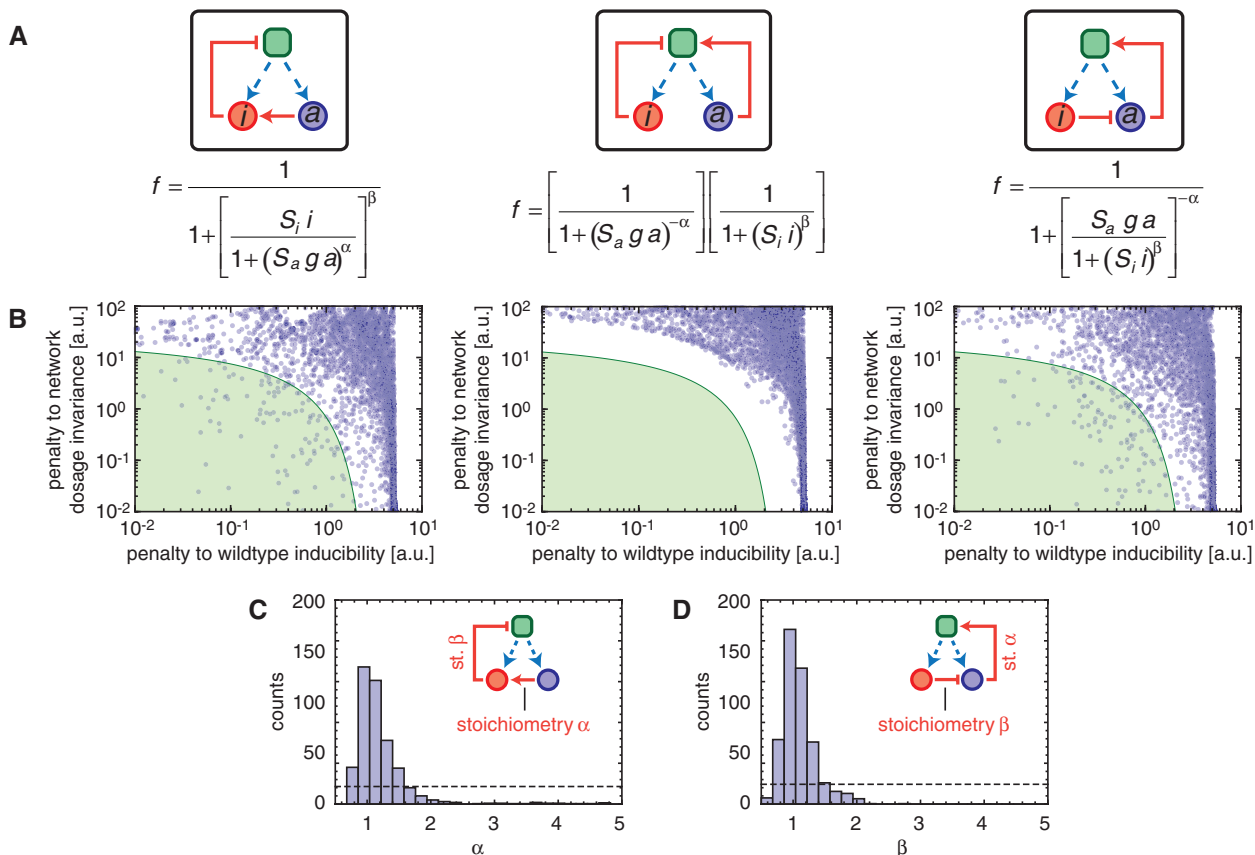


Fig. 4. Numerical analysis of general network features producing an inducible and network-dosage invariant system. **(A)** Each functional form represents the relationship between the fraction of transcriptionally active cells and the total concentrations of the activating (*a*) and inhibiting (*i*) agents. Blue and red circles represent activating and inhibiting agents, respectively. Dashed blue arrows denote the transcriptional production of the network components. The green square represents a transcriptional center. Pointing red arrows show direct activation, whereas blunt red arrows represent inhibition. Each configuration is described by four parameters: the scales of action of the activator and inhibitor (S_a and S_i ,

respectively) and coefficients (α and β) quantifying the typical nonlinearity of the interaction with downstream components. **(B)** For each configuration depicted in **(A)**, the degree of inducibility and network-dosage invariance of systems are plotted on the *x* and *y* axes, respectively. The green region corresponds to systems that are both inducible and network-dosage invariant. **(C)** For the left configuration in **(A)**, histogram of the parameter values corresponding to the green region shown in **(B)**. **(D)** As in **(C)** but for the right configuration shown in **(A)**. In **(C)** and **(D)**, the dotted lines show what one would expect had the parameters had no effect in determining whether the system was in the green region or not.

inhibitor. However, given the nonlinear effect of each component on output, compensation cannot be maintained over a large range of input levels. The system thus fails to be both inducible and network-dosage invariant. For the other systems analyzed, when the one-to-one stoichiometry condition is satisfied, an increase in the activator concentration is compensated by an increase in the inhibitor, because the regulation function is dependent on just the ratio of these levels (15).

The network-dosage invariant GAL system satisfies the dosage compensation requirements identified by the minimal model: The interaction topology between its activator (*GAL3*) and inhibitor (*GAL80*) is similar to the topology depicted in Fig. 4, left. In addition, it has been experimentally shown (16) that *GAL3* and *GAL80* interact with one-to-one stoichiometry. These observations further validate our findings.

By using a constitutive promoter (*CYCI*) to eliminate the feedback regulation through the *GAL3* and *GAL80* genes, earlier work (17) measured the contribution of the *GAL3* and *GAL80*

feedback loops to the noise in the network activity. It was found that without the feedback regulation the activity of the GAL network became noisier compared with activity of the wild-type network. Here, we have kept feedback regulation intact by maintaining at least one copy of the *GAL3* and *GAL80* genes and probed the effect of gene and network-dosage variations on the network activity, elucidating the contribution of network structure on dosage compensation.

These results provide a volume-independent mechanism that is sufficient for network-dosage invariance. The mechanism requires at least two network components: one positive and one negative regulator. These components have to interact with a one-to-one effective stoichiometry and have specific topologies allowing only one of them to directly affect transcription. This type of interaction topology is frequently observed (18–21) in natural gene circuits that use sequestration-based signal transduction schemes. Robust network properties such as network-dosage invariance might be selected over evolutionary time scales;

therefore, network-dosage invariance could represent a general design principle for gene network architecture in cells (22–29).

References and Notes

1. J. A. Lee, J. R. Lupski, *Neuron* **52**, 103 (2006).
2. T. Galitski, A. J. Saldanha, C. A. Styles, E. S. Lander, G. R. Fink, *Science* **285**, 251 (1999).
3. S. Di Talia *et al.*, *PLoS Biol.* **7**, e1000221 (2009).
4. M. Kellis, B. W. Birren, E. S. Lander, *Nature* **428**, 617 (2004).
5. G. Rancati *et al.*, *Cell* **135**, 879 (2008).
6. J. M. Pedraza, A. van Oudenaarden, *Science* **307**, 1965 (2005).
7. M. Acar, A. Becskei, A. van Oudenaarden, *Nature* **435**, 228 (2005).
8. T. S. Gardner, C. R. Cantor, J. J. Collins, *Nature* **403**, 339 (2000).
9. W. Xiong, J. E. Ferrell Jr., *Nature* **426**, 460 (2003).
10. A. Mizutani, M. Tanaka, *EMBO J.* **22**, 2178 (2003).
11. K. Melcher, H. E. Xu, *EMBO J.* **20**, 841 (2001).
12. T. Suzuki-Fujimoto *et al.*, *Mol. Cell. Biol.* **16**, 2504 (1996).

13. G. Peng, J. E. Hopper, *Mol. Cell. Biol.* **20**, 5140 (2000).
 14. G. Peng, J. E. Hopper, *Proc. Natl. Acad. Sci. U.S.A.* **99**, 8548 (2002).
 15. Materials and methods are available as supporting material on Science Online.
 16. D. J. Timson, H. C. Ross, R. J. Reece, *Biochem. J.* **363**, 515 (2002).
 17. S. A. Ramsey *et al.*, *Nat. Genet.* **38**, 1082 (2006).
 18. N. E. Buchler, M. Louis, *J. Mol. Biol.* **384**, 1106 (2008).
 19. L. Bardwell *et al.*, *Genes Dev.* **12**, 2887 (1998).
 20. Y. Liu, J. M. Belote, *Mol. Gen. Genet.* **248**, 182 (1995).
 21. R. Benezra, R. L. Davis, D. Lockshon, D. L. Turner, H. Weintraub, *Cell* **61**, 49 (1990).
 22. H. Kacser, J. A. Burns, *Symp. Soc. Exp. Biol.* **27**, 65 (1973).
 23. M. Kollmann, L. Løvdok, K. Bartholomé, J. Timmer, V. Sourjik, *Nature* **438**, 504 (2005).
 24. D. Fell, *Understanding the Control of Metabolism* (Portland, London, 1997).
 25. U. Alon, M. G. Surette, N. Barkai, S. Leibler, *Nature* **397**, 168 (1999).
 26. A. Eldar *et al.*, *Nature* **419**, 304 (2002).
 27. G. Shinar, R. Milo, M. R. Martínez, U. Alon, *Proc. Natl. Acad. Sci. U.S.A.* **104**, 19931 (2007).
 28. M. A. Savageau, *Nature* **252**, 546 (1974).
 29. U. Alon, *An Introduction to Systems Biology: Design Principles of Biological Circuits* (Chapman & Hall, Boca Raton, FL, 2007).
 30. The authors would like to thank J. J. Collins, M. Thattai, and H. Youk for helpful discussions and/or comments on

the manuscript. M.A. was supported by a fellowship grant from the Center for Biological Circuit Design at Caltech. B.F.P. and A.v.O. were supported by grants from NIH and NSF. Work in the Elowitz laboratory was supported by the Packard Foundation, NSF, and NIH. Work in the Arnold laboratory was supported by NIH.

Supporting Online Material

www.sciencemag.org/cgi/content/full/329/5999/1656/DC1
 Materials and Methods
 Figs. S1 to S8
 Tables S1 to S5
 References and Notes

6 April 2010; accepted 9 August 2010
 10.1126/science.1190544

A *Vibrio* Effector Protein Is an Inositol Phosphatase and Disrupts Host Cell Membrane Integrity

Christopher A. Broberg, Lingling Zhang, Herman Gonzalez, Michelle A. Laskowski-Arce, Kim Orth*

The marine bacterium *Vibrio parahaemolyticus* causes gastroenteritis in humans and encodes the type III effector protein VPA0450, which contributes to host cell death caused by autophagy, cell rounding, and cell lysis. We found that VPA0450 is an inositol polyphosphate 5-phosphatase that hydrolyzed the D5 phosphate from the plasma membrane phospholipid phosphatidylinositol 4,5-bisphosphate. VPA0450 disrupted cytoskeletal binding sites on the inner surface of membranes of human cells and caused plasma membrane blebbing, which compromised membrane integrity and probably contributed to cell death by facilitating lysis. Thus, bacterial pathogens can disrupt adaptor protein-binding sites required for proper membrane and cytoskeleton dynamics by altering the homeostasis of membrane-bound inositol-signaling molecules.

The Gram-negative marine bacterium *Vibrio parahaemolyticus* is a leading cause of gastroenteritis from the consumption of contaminated seafood (1). Many virulent strains of *V. parahaemolyticus* encode thermostable direct hemolysins and two type III secretion systems (T3SS1 and T3SS2) (2, 3). The T3SS is

a syringe-like mechanism often used by Gram-negative bacteria to introduce effector proteins into eukaryotic target cells during infection (4).

The *V. parahaemolyticus* T3SS1 injects effectors that cause a rapid, orchestrated cell death mediated by autophagy, cell rounding, and then cell lysis (5). One effector, VopQ, is both nec-

essary and sufficient to induce autophagy (6), whereas another effector, VopS, is an AMPylator that contributes to cell rounding by modifying a conserved threonine residue on the Rho family of guanosine triphosphatases (GTPases) with adenosine 5'-monophosphate (AMP), preventing their interaction with downstream-signaling molecules (7). Upon analysis of the contribution of other T3SS1 effectors (8) involved in this paradigm of cell death, we found that a strain with only a functional T3SS1 (POR3) that was deleted for the effector VPA0450 (POR3Δ*vpa0450*) (Fig. 1B and fig. S1A) caused cell rounding faster than the parental POR3 strain or the complemented strain (POR3Δ*vpa0450* + VPA0450) during infection of HeLa cells (Fig. 1, A and C, respectively) (9). Additionally, both the POR3 strain (Fig. 1, E and I) and the complemented POR3Δ*vpa0450* + VPA0450 strain (Fig. 1, G and J) induced a transient blebbing of the host cell membrane before cell rounding, whereas POR3Δ*vpa0450* initiated rounding without any blebbing (Fig. 1, B and F). Further analysis revealed that POR3Δ*vpa0450* delayed lysis of the infected cell by approximate-

Department of Molecular Biology, University of Texas Southwestern Medical Center, Dallas, TX 75390, USA.

*To whom correspondence should be addressed. E-mail: kim.orth@utsouthwestern.edu

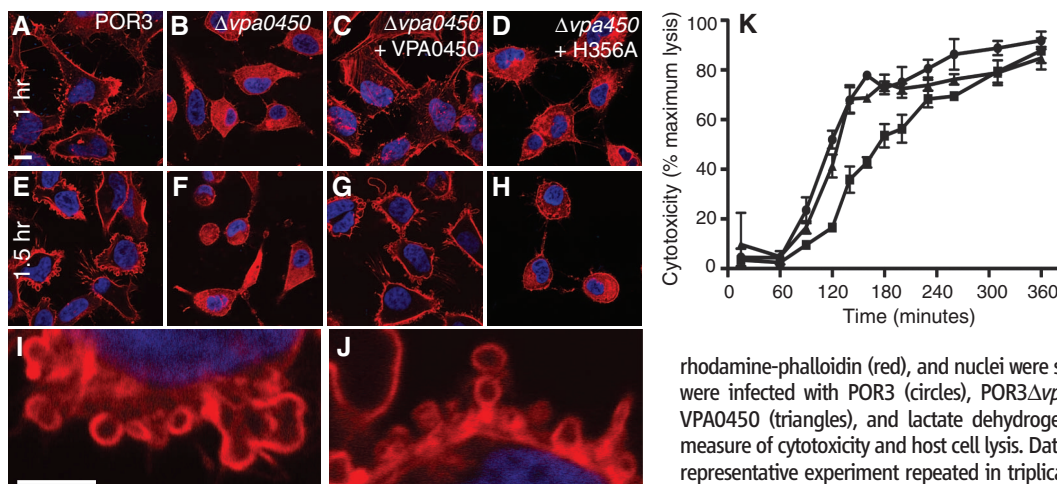


Fig. 1. Expression of VPA0450 leads to rapid host cell lysis. HeLa cells were infected with POR3, POR3Δ*vpa0450*, POR3Δ*vpa0450* + VPA0450, or POR3Δ*vpa0450* + VPA0450-H356A and visualized with confocal microscopy at, respectively, (A to D) 1 hour and (E to H) 1.5 hours. Scale bar, 10 μm. Blebbing is shown in detail from (I) POR3 and (J) POR3Δ*vpa0450* + VPA0450 infection at 1.5 hours. Scale bar, 5 μm. Actin cytoskeleton was stained with rhodamine-phalloidin (red), and nuclei were stained with Hoechst (blue). (K) HeLa cells were infected with POR3 (circles), POR3Δ*vpa0450* (squares), or POR3Δ*vpa0450* + VPA0450 (triangles), and lactate dehydrogenase (LDH) release was evaluated as a measure of cytotoxicity and host cell lysis. Data are means ± SD (n = 3 samples) from a representative experiment repeated in triplicate.